Arch. Metall. Mater. **63** (2018), 2, 1043-1047

DOI: 10.24425/122440

X.-K. HUYNH*, B.-W. KIM** J.-S. KIM***#

FABRICATION OF Fe-TiB_2 NANOCOMPOSITES BY SPARK-PLASMA SINTERING OF A (FeB, TiH_2) POWDER MIXTURE

Fe-40wt% TiB_2 nanocomposites were fabricated by mechanical activation and spark-plasma sintering of a powder mixture of iron boride (FeB) and titanium hydride (TiH_2). The powder mixture of (FeB, TiH_2) was prepared by high-energy ball milling in a planetary ball mill at 700 rpm for 3 h followed by spark-plasma sintering (SPS) at various conditions. Analysis of the change in relative sintered density and densification rate during sintering showed that a self-propagating high-temperature synthesis reaction occurs to form TiB_2 from FeB and Ti. A sintered body with relative density higher than 98% was obtained after sintering at 1150°C for 5 and 15 min. The microstructural observation of sintered compacts with the use of FE-SEM and TEM revealed that ultrafine particulates with approximately 5 nm were evenly distributed in an Fe-matrix. A hardness value of 83 HRC was obtained, which is equivalent to that of conventional WC-20 Co systems.

Keywords: Fe-TiB_2 nanocomposite, mechanical activation, spark-plasma sintering, self-propagating high-temperature synthesis reaction

1. Introduction

The Fe-TiB_2 composite has attracted much attention due to its excellent mechanical properties. Many researchers have reported synthesis methods for the TiB_2 phase by various methods: laser cladding [1,2], plasma transferred arc (PTA) [3,4], aluminothermic reduction [5], spark plasma sintering (SPS) [6], and self-propagating high-temperature synthesis (SHS) [7-10]. Most of these reports did not show homogenous distribution of dispersoids with a fine particle size. Additionally, many of them used only pure elements or elemental powders as starting materials, even though they had an unfavorable cost.

It is well known that an in situ technique has many advantages for fabricating composite materials. The in situ process involves synthesizing the reinforcing phase within a matrix during the fabrication process by a chemical reaction between elements or compounds. In situ formation can bring positive results for additional processes such as reduction of reinforcement size with a narrow distribution, even dispersion of reinforcements, and a clean interface between the reinforcement-matrix with high interfacial strength [11]. In a previous work, we reported that Fe-TiB_2 nanocomposite powder with TiB_2 particulates smaller than 5 nm could be fabricated by an in situ method using FeB and TiH_2 as starting powders [12].

We reported the results of pressureless-sintering of (FeB, TiH_2) powder compacts [13]. Full densification could not be obtained, and the size of the TiB_2 particulates in the Fe-matrix grew to several micrometers, even though the microstructure still showed a homogenous dispersion of TiB_2 particulates in the Fe-matrix. To exploit the advantages of nanocomposite powders, the size of the reinforcements should be kept to nanoscale during or after further sintering. In this sense, the spark plasma sintering process is well known as one of the most effective sintering techniques, especially for nanocomposites [14].

The aim of the present work is to investigate the feasibility of fabricating nanosize-TiB_2-reinforced Fe matrix composite by spark-plasma sintering of a high-energy ball-milled powder mixture of FeB and TiH_2.

2. Experimental procedure

A composite with a composition of Fe-40 wt% TiB_2 (52 vol%) was fabricated from FeB and TiH_2 starting powders. The (FeB, TiH_2) powder mixture was ground in a planetary ball mill for 3 hours at 700 rpm before using for sintering investigation. More details of the fabrication process of the (FeB, TiH_2) powder mixture can be found in our previous works [12,15].

Spark plasma sintering was performed using the SPS-515S system (Sumitomo Coal Mining Co., Japan). The as-milled powder mixtures were loaded into cylindrical graphite dies and heated at a rate of 50°C/min. The sintering temperature was varied in a range of 1000°C and 1150°C. A constant pressure of 50 MPa in a vacuum chamber was applied for all experiments.

* INDUSTRIAL UNIVERSITY OF HO CHI MINH CITY, FACULTY OF MECHANICAL TECHNOLOGY, HO CHI MINH CITY, VIETNAM
** UNIVERSITY OF ULSAN, SCHOOL OF ELECTRICAL ENGINEERING, ULSAN 44610, REPUBLIC OF KOREA
*** UNIVERSITY OF ULSAN, SCHOOL OF MATERIALS SCIENCE AND ENGINEERING, ULSAN 44610, REPUBLIC OF KOREA
\# Corresponding author: jskim@ulsan.ac.kr

The data, including shrinkage, temperature, vacuum condition, pulse voltage and current, were digitaly stored by a data acquisition system and used for further analysis.

The phase for the sintered compacts was analyzed by a X-ray diffractometer (XRD) using CuKα radiation. The microstructure was observed and analyzed with a field-emission scanning electron microscope (FE-SEM) and high-resolution transmission electron microscope (HR-TEM). HR-TEM micrographs were filtered using an inverse Fourier fast transform (FFT) program in Gatan Digital Micrography software to confirm the exact fringe spacing of the precipitated nanoparticles.

Hardness values of all sintered composites were measured by Vickers's method with a 2 kg load (19.6N, HV_2), and the values were converted to Rockwell Hardness (HRC).

3. Results and discussion

Figure 1 shows the change in relative density (RD) and densification rate during the spark-plasma sintering process. The (FeB, TiH_2) powder compact was heated to 1150°C at a heating rate of 50°C/min under a sintering pressure of 50 MPa and then held for 15 min. The relative density curve showed two rapid densification events near 700°C and 1000°C. These two fast densification events were clear on the densification rate curve.

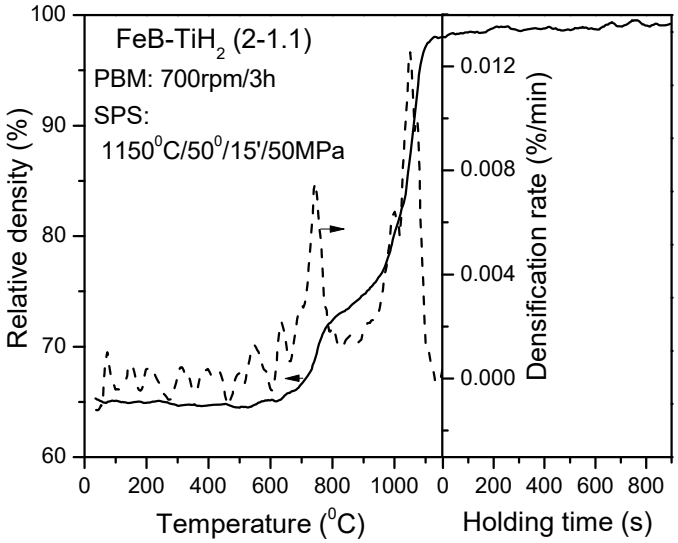

Fig. 1. Change of relative density (RD) and densification rate during the spark-plasma sintering process. The (FeB, TiH_2) powder compact was heated to 1150°C at a heating rate of 50°C/min under a sintering pressure of 50 MPa and then held for 15 min

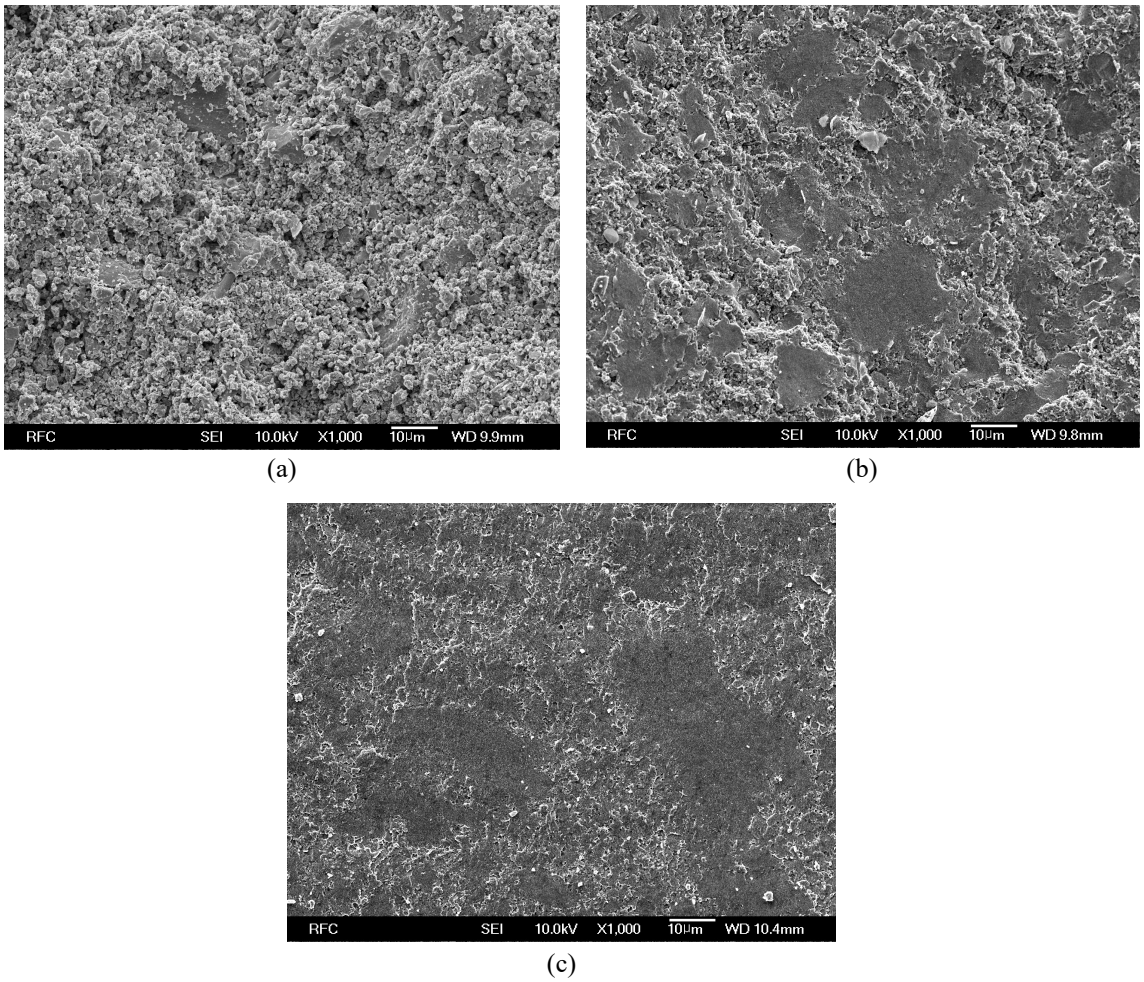

Fig. 2. FE-SEM secondary-electron images of the fractured surfaces of FBT powder compacts spark-plasma sintering at various temperature: (a) 1000°C (79% relative density, RD), (b) 1070°C (90% RD), and (c) 1150°C (98% RD) for 0 min

The first peak on the densification rate curve was found between 700°C and 800°C. This peak seems to be a result of the in situ synthesis of nanoscale TiB_2 between Ti from TiH_2 and B in FeB under the following equation, as already reported in our previous works [12,13].

$$2FeB(s) + TiH_2(s) \rightarrow 2Fe(s) + TiB_2(s) + H_2(g) \uparrow$$

The second peak on the densification rate curve is located in the range of 1000-1100°C. The densification proceeded fast and resulted in a high sintered density of 97% even at 1100°C. Further heating with a holding time brought only a small increase in sintered density up to 98%.

To investigate the sintering behavior more clearly, the fracture surfaces of some selected sintered compacts were observed by FE-SEM. The results are shown in Fig. 2. As discussed above, the highest increase in densification rate started near 1000°C. The specimen sintered at 1000°C showed a sintered density of 79%, a microstructure composed of mostly pores, and neck areas partly formed between agglomerates, which led to an easy fracture. The further increase of sintering temperature up to 1070°C enhanced the densification process. The sintered density increased drastically to 90% RD, and the microstructure changed to a larger neck area. A nearly full density of 98% was obtained at 1150°C. Considering our previous results from pressureless-sintering of the same powder mixture of (FeB, TiB_2) [13], the effectiveness of the spark-plasma sintering process is evident. We obtained a maximum sintered density of 96% RD even after pressureless-sintering at 1400°C for 2 hours.

XRD patterns of selected sintered compacts are given in Fig. 3. It is evident that two phases of Fe and TiB_2 exist in all sintered compacts, except the compact sintered at 800°C for 15 min. Additionally, the samples sintered at 1150°C for 15 min showed the TiB phase in addition to both of these phases. These results are nearly the same as reported in our previous work on pressureless-sintering [13]. The excess Ti seems to react with TiB_2 again to form the TiB phase at high temperature after formation at lower temperature [16,17]. The SHS reaction during the SPS process seemed to occur between 800°C and 1050°C.

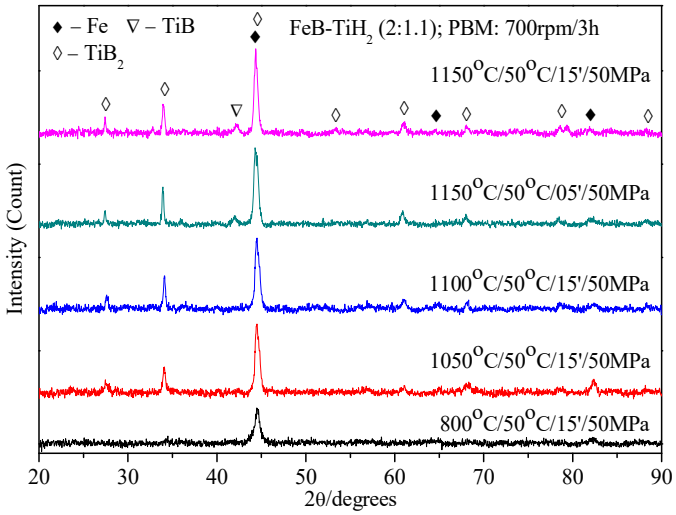

Fig. 3. XRD patterns of (FeB, TiH_2) powder compacts sintered by spark-plasma sintering at various sintering conditions (Sintering temperature/ Heating rate/Sintering time/Sintering pressure)

The polished cross-section of (FeB, TiB_2) powder compacts sintered at 1150°C for 5 and 15 min were observed with FE-SEM. Their backscattered-electron images are given in Fig. 4. The nanoscale dark-grey TiB_2 particulates were homogeneously distributed in the relatively bright Fe-matrix. An increase in sintering time from 5 min to 15 min did not result in higher sintered density, but did increase the growth of TiB_2 particulates up to several hundreds of nanometers. The effectiveness of spark-plasma sintering should be noted again: in the case of pressureless-sintering of the same powder [13], the growth of TiB_2 particulates occurred more strongly up to several micrometers due to a long holding time at high sintering temperature.

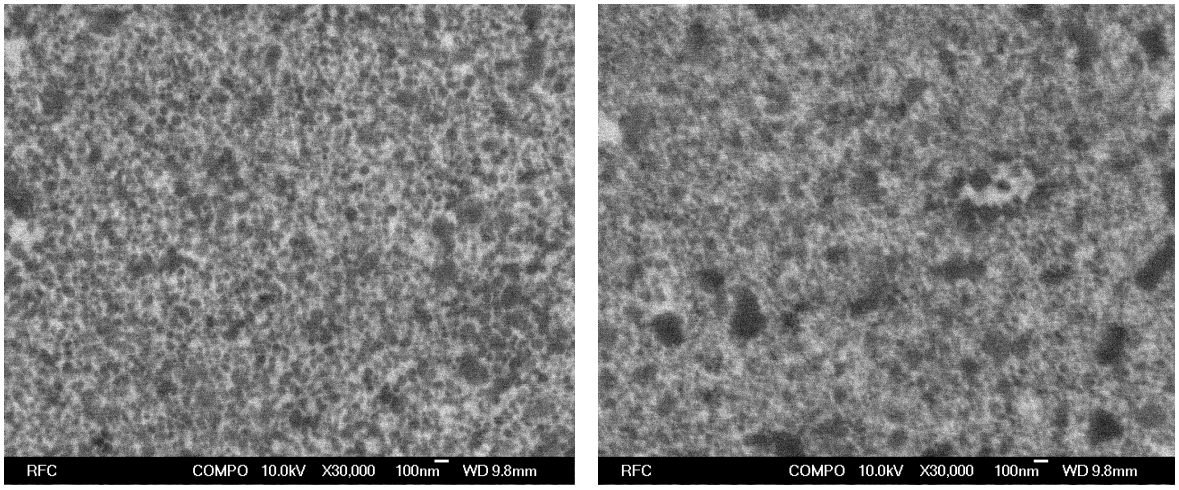

(a) (b)

Fig. 4. FE-SEM backscattered-electron images of the polished cross-section of (FeB, TiH_2) powder compacts sintered at 1150°C for (a) 5 min. (98% RD) and (b) 15 min. (98% RD)

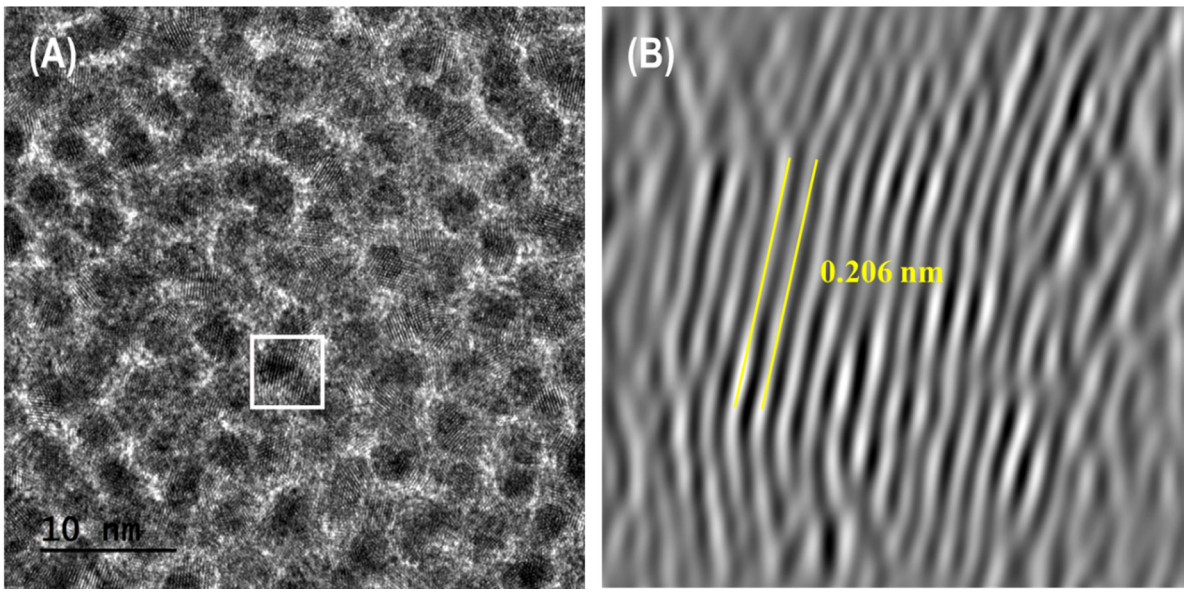

Fig. 5. (a) High resolution TEM image of (FeB, TiH_2) powder compacts sintered at 1150°C for 15 min and (b) the inverse Fast-Fourier Transferred (FFT) image reconstructed from the selected area marked by the white square

To identify the existence and size of TiB_2 particulates in the sintered compact, an HR-TEM image was obtained with an inverse Fast-Fourier Transferred (FFT) image, as shown in Fig. 5. Figure 5b shows the inverse Fast-Fourier Transferred (FFT) image reconstructed from the mask-applied FFT image of the selected area (white square) shown in the HR-TEM image of Fig. 5a. The fringe spacing of 0.206 nm was measured from this image. This value corresponds to the interplanar spacing between (101) planes of TiB_2. Approximately 5 nm TiB_2 particulates were evenly dispersed in the Fe-matrix.

Figure 6 shows the relationship between hardness and sintered density. It is evident that the increase in sintered density led to an increase in hardness. However, the increase of sintering time at 1150°C from 5 min to 15 min did not lead to an increase in sintered density but to the growth of TiB_2 particulates. The lower hardness for the latter can be explained by the difference in microstructure by this effect. Fairly high hardness values of 78.4-83.7 HRC were obtained from all sintered compacts with a density greater than 95% RD, even though the Fe-TiB_2 nanocomposite fabricated in this study contained 60 wt.% Fe. Conventional WC-Co hardmetals containing 20 wt.% Co were approximately 70 HRC [14]. The reason for such a high hardness value seems to be a result of the homogeneous distribution of ultrafine TiB_2 particulates and the sound interface between TiB_2 particulates and Fe matrix.

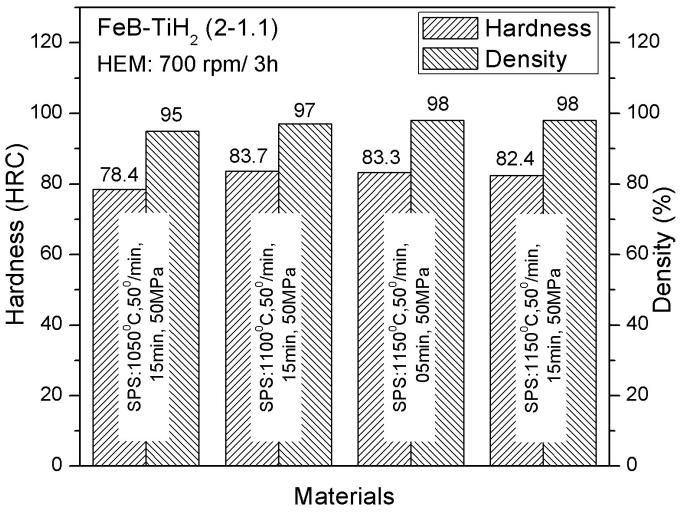

Fig. 6. Hardness and sintered density of (FeB, TiH_2) powder compacts sintered at various spark-plasma sintering conditions

4. Conclusions

The feasibility tests for fabrication of Fe-TiB_2 nanocomposites were performed by spark-plasma sintering of the (FeB, TiH_2) powder mixture prepared by high-energy ball-milling. From the results of the sintering behavior, X-ray phase analysis, observation, analysis of the microstructure using FE-SEM and EDS, and hardness measurements, the following were concluded:

(1) The effectiveness of the spark-plasma sintering was confirmed. A nearly full relative density of 98% was obtained, even at a much low sintering temperature of 1150°C and a shorter sintering time of 5-15 min, in comparison to our previous works on pressureless-sintering, where only a maximum 96% relative density was obtained after sintering at 1400°C for 2 hours.

(2) The densification rate increased drastically in two separate temperature ranges of 700-800°C and 1000-1100°C. The first seems to be a result of the self-propagating high-temperature synthesis reaction between Ti from TiH_2 and B in FeB to form TiB_2. The second is from the normal densification behavior enhanced by the spark-plasma sintering effect.

(3) The sintered compacts have the two main phases of Fe and TiB_2 with a trace of TiB, which seems to be formed through the reaction of TiB_2 formed at lower temperature during the heating stage and excess Ti that was intentionally added for a complete reaction of TiB_2 formation.

(4) The fully densified sintered compacts with 98% RD show homogeneous microstructures composed of ultrafine TiB_2 particulates of 5 nm size evenly dispersed in a Fe-matrix.

(5) Hardness values of 82.4-83.7 HRC were obtained from sintered compacts greater than 97% RD, which was much higher than conventional WC-Co hardmetals containing 20 wt.% Co.

Acknowledgements

This work was supported by the 2016 Research Fund of University of Ulsan.

REFERENCES

[1] B. Du, Z. Zou, X. Wang, S. Qu, Appl. Surf. Sci. **254**, 6489-6494 (2008).

[2] B. Du, Z. Zou, X. Wang, S. Qu, Mat. Lett. **62**, 689-691 (2008).

[3] M. Darabara, G.D. Papadimitriou, L. Bourithis, Surf. Coat. Technol. **201**, 3518-3523 (2006).

[4] W. Xibao, W. Xiaofeng, S. Zhongquan, Surf. Coat. Technol. **192**, 257-262 (2005).

[5] A. Anal, T.K. Bandyopadhyay, K. Das, J. Mater. Process. Technol. **172**, 70-76 (2006).

[6] B. Li, Y. Liu, H. Cao, L. He, J. Li, J. Mater. Sci. **44**, 3909-3912 (2009).

[7] O.K. Lepakova, L.G. Raskolenko, Y.M. Maksimov, Combust. Explos. Shock Waves **36**, 575-581 (2000).

[8] C.C. Degnan, P.H. Shipway, Metall. Mater. Trans. A **33**, 2973-2983 (2002).

[9] L. Gai, M. Ziemnicka-Sylwester, Int. J. Refract. Met. Hard Mater. **45**, 141-146 (2014).

[10] O.K. Lepakova, L.G. Raskolenko, Y.M. Maksimov, J. Mater. Sci. **39**, 3723-3732 (2004).

[11] R.M. Aikin, JOM **49**, 35-39 (1997).

[12] X.K. Huynh, S.W. Bae, J.S. Kim, Korean J. Met. Mater. **55**, 10-15 (2017).

[13] X.K. Huynh, J.S. Kim, J. Korean Powder Metall. Inst. **23**, 282-286 (2016).

[14] N. Saheb, Z. Iqbal, A. Khalil, A.S. Hakeem, N.A. Aqeeli, T. Laoui, A. Al-Qutub, R. Kirchner, Journal of Nanomaterials **2012**, Article ID 983470, 13 pages (2012).

[15] X.K. Huynh, Fabrication of Fe-TiB2 Nanocomposite with Use of High-energy Milling Followed by in situ Reaction Synthesis and Sintering, PhD Thesis, University of Ulsan, Ulsan, Korea

[16] O.K. Lepakova, L.G. Raskolenko, Y.M. Maksimov, Combust. Explos. Shock Waves **36**, 575-581 (2000).

[17] C.C. Degnan, P.H. Shipway, Metall. Mater. Trans. A **33**, 2973-2983 (2002).